OXFORD

Cerebral Cortex, 2022, 1–15
https://doi.org/10.1093/cercor/bhac384
Original Article

Sustained upregulation of widespread hippocampal–neocortical coupling following memory encoding

Line Folvik[1,*], Markus H. Sneve[1], Hedda T. Ness[1], Didac Vidal-Piñeiro[1], Liisa Raud[1], Oliver M. Geier[2], Kristine B. Walhovd[1,3], Anders M. Fjell[1,3]

[1]Department of Psychology, Center for Lifespan Changes in Brain and Cognition, University of Oslo, Forskningsveien 3A, 0373 Oslo, Norway,
[2]Department of Diagnostic Physics, Oslo University Hospital, Postbox 4950 Nydalen, OUS, Rikshospitalet, 0424 Oslo, Norway,
[3]Division of Radiology and Nuclear Medicine, Oslo University Hospital, Postbox 4950 Nydalen, OUS, Rikshospitalet, 0424 Oslo, Norway
*Corresponding author: Department of Psychology, University of Oslo, Oslo 0373, Norway. Email: line.folvik@psykologi.uio.no

Systems consolidation of new experiences into lasting episodic memories involves hippocampal–neocortical interactions. Evidence of this process is already observed during early post-encoding rest periods, both as increased hippocampal coupling with task-relevant perceptual regions and reactivation of stimulus-specific patterns following intensive encoding tasks. We investigate the spatial and temporal characteristics of these hippocampally anchored post-encoding neocortical modulations. Eighty-nine adults participated in an experiment consisting of interleaved memory task- and resting-state periods. We observed increased post-encoding functional connectivity between hippocampus and individually localized neocortical regions responsive to stimuli encountered during memory encoding. Post-encoding modulations were manifested as a nearly system-wide upregulation in hippocampal coupling with all major functional networks. The configuration of these extensive modulations resembled hippocampal–neocortical interaction patterns estimated from active encoding operations, suggesting hippocampal post-encoding involvement exceeds perceptual aspects. Reinstatement of encoding patterns was not observed in resting-state scans collected 12 h later, nor when using other candidate seed regions. The similarity in hippocampal functional coupling between online memory encoding and offline post-encoding rest suggests reactivation in humans involves a spectrum of cognitive processes engaged during the experience of an event. There were no age effects, suggesting that upregulation of hippocampal–neocortical connectivity represents a general phenomenon seen across the adult lifespan.

Key words: hippocampus; functional connectivity; fMRI; reactivation; systems consolidation.

Introduction

Memory systems consolidation refers to the transformation of experiences into longer-lasting episodic memories via hippocampal–neocortical interactions (Alvarez and Squire 1994; Nadel and Moscovitch 1997). Animal research suggest that such stabilization of memory traces results from spontaneous reactivations of hippocampal–neocortical connectivity patterns, which can occur both during deep sleep (O'Neill et al. 2010) and awake periods of rest (Carr et al. 2011). Due to its spontaneous nature, it is difficult to achieve adequate experimental control of systems consolidation resulting from hippocampal reactivation. In recent years, however, task-free functional magnetic resonance imaging (fMRI) and magnetoencephalography (MEG) have been used successfully to investigate reactivation-related processes in awake humans noninvasively and with high spatial precision (Kurth-Nelson et al. 2016; Liu et al. 2019; Tambini and Davachi 2019). Several fMRI studies have found experience-dependent alterations in resting-state functional connectivity (rsFC) between hippocampus and category-sensitive cortices after an encoding task compared to a pre-encoding baseline measure (Tambini et al. 2010; Schlichting and Preston 2014; de Voogd et al. 2016; Murty et al. 2017). While most rsFC studies have focused on hippocampal interactions with pre-defined, task-relevant perceptual regions, investigations in nonhuman primates (Logothetis et al. 2012), and recently in humans using MEG (Higgins et al. 2021), have shown that hippocampal states associated with reactivation and memory consolidation coincide with activity modulations in large parts of the neocortex, also beyond sensorimotor and perceptual cortices. Currently, however, we do not know whether these extensive neocortical modulations are part of a system-wide upregulation of hippocampal functional connectivity during post-encoding periods. Alternatively, hippocampal functional modulations could be limited to category-selective cortex while engagement of non-sensory networks could occur via alternative pathways, e.g. mediated by the thalamus (Wagner et al. 2019). Critically, hippocampal functional connectivity modulations during memory-relevant task states involve large portions of the neocortex (McCormick et al. 2010; Sneve et al. 2015; Westphal et al. 2017; King et al. 2018; Cooper and Ritchey 2019; Tang et al. 2020; Beason-Held et al. 2021). If these broader hippocampal networks are coordinated similarly also during post-encoding rest, this would suggest state continuation into periods without systematic exposure to

Received: February 11, 2022. **Revised:** August 29, 2022. **Accepted:** August 30, 2022

Table 1. Sample characteristics.

	Young adults			Older adults		
	n	Mean (SD)	Range	*n*	Mean (SD)	Range
Age	47	26.5 (4.20)	20–38	42	67.1(5.81)	60–81
MMSE[a]	46	29 (1.07)	27–30	42	29.1 (1.07)	27–30
IQ[a]	46	110 (8.97)	90–125	41	121 (9.84)	90–146
Education[b]	45	15.2(2.02)	13–18	39	16.3 (2.06)	10–21

[a]MMSE and IQ scores were missing for one older participant and IQ score was missing for one younger participant who could not complete testing due to COVID-19 restrictions. [b]Education = years of total education rounded down to the closest whole number.

external stimuli—akin to system-wide maintenance or "reactivation" of memory-relevant interactions between brain regions. With few exceptions (Kukolja et al. 2016), studies on the effect of age on awake systems consolidation processes are sparse. Age is among the strongest individual predictors of episodic memory function, and the memory decline observed in normal aging is related to changes in hippocampal structure and function (Nyberg et al. 2012). By including participants with higher age, potential age effects could indicate whether changes in awake post-encoding interactions are related to the commonly observed memory reductions in aging.

In the present fMRI study, we characterized the systems-level changes in hippocampal interactions occurring in humans following an intense learning session. Younger and older adults ($N = 89$; Table 1) completed an intentional associative memory encoding task involving stimulus categories for which there exist established functional localizers. Reactivation-related changes in hippocampal–neocortical rsFC were estimated from resting-state periods taking place immediately before and after the encoding task as well as after a delay of 12 h (Fig. 1). We ran additional localizer sequences to individually map object-, face-, and place-sensitive regions. Our first aim was to replicate previous reports of increased post-encoding rsFC between hippocampus and these category-sensitive perceptual regions. Importantly, we also tested for reactivation effects outside stimulus-selective cortex, both exploratory at the whole-brain parcel level and at the level of established "canonical" resting-state networks. Post-encoding modulations in hippocampal rsFC were compared with functional connectivity patterns estimated from encoding and retrieval task periods. Strong resemblance with encoding patterns would support an interpretation of ongoing reactivation (Tambini and Davachi 2019). Higher similarity with retrieval patterns, on the other hand, could indicate rehearsal-like operations and would potentially invalidate an interpretation of post-encoding rsFC modulations as reflective of spontaneous consolidation processes in the awake state. Finally, the current sample consisted of younger and older adults. Throughout the analyses, we systematically tested whether awake hippocampal rsFC modulations were affected by participant age.

Materials and methods

Participants

Ninety-two participants were enrolled in the present study: 49 younger (20–38 years; 25 females) and 43 older adults (60–80 years; 25 females). All participants were fluent in Norwegian, right-handed, with normal or corrected vision and no history of severe psychiatric or neurological disorder, traumatic or enhanced brain injury, and no current use of medications known to affect the nervous system. Included participants were required to score ≥26 on the Mini-Mental State Examination (MMSE; Folstein et al. 1975), have normal intelligence quotient (IQ) or above (IQ ≥ 85) measured with the Wechsler Abbreviated Scale of Intelligence (Wechsler 1999), and no major depression indicated by the Beck Depression Inventory (Beck et al. 1988) or the Geriatric Depression Scale (Yesavage et al. 1982). See characteristics of the final sample in Table 1. All participants signed an informed consent approved by the Regional Ethical Committee of South Norway. The main recruiting strategies included targeted Social Media advertisement, flyers, and posters at selected places (e.g. senior centers). Participants were compensated for the participation.

Experimental design

This study is part of a larger project investigating memory consolidation processes at different time scales and their possible relation to memory decline in aging (https://cordis.europa.eu/project/id/725025). Relevant sessions for this report include an fMRI paradigm consisting of 12 min baseline/pre-encoding resting-state fMRI (rsfMRI) before 2 runs of an associative encoding task (12 min each), immediately followed by 12 min post-encoding rsfMRI. Then, approximately 20 min after the end of the last encoding run, a forced-choice memory test was administered outside the scanner. Following a 12-h interval, participants returned for another post-encoding rsfMRI scan before performing 3 runs of a retrieval task in the scanner (12 min each). Additionally, 4 functional localizer runs (6 min each), enabling localization of regions sensitive to stimulus categories presented during the encoding task, and several structural scans were performed. A second and third forced-choice memory tests were administered ∼12 h and ∼5 days post-encoding, respectively. The participants also underwent a session of neuropsychological testing (∼3 h) and several questionnaires. The described structure is depicted in Fig. 1.

Eighty-three of the 92 participants completed the fMRI paradigm 2 times, resulting in 175 sessions. The 2 visits were separated at least 6 days apart, with unique sets of task stimuli at each visit. Fifteen sessions had to be excluded for the following reasons: one session from 11 participants was excluded as they reported rehearsing the encoded associations during the post-encoding rest; one of these (a young male) had only one visit and was excluded entirely. Additionally, one session from 2 participants was excluded due to an interruption between encoding and post-encoding rest. One older male was excluded based on motion (mean framewise displacement > 0.2). One young male participant was excluded due to the suspicion that he fell asleep during post-encoding rest scans. Final sample for further analysis was 89 unique participants and 158 sessions. The visits were characterized by either having the encoding task administered in the morning (8–10 AM) ($n = 79$) or in the evening (8–10 PM) ($n = 79$). For the morning encoding session,

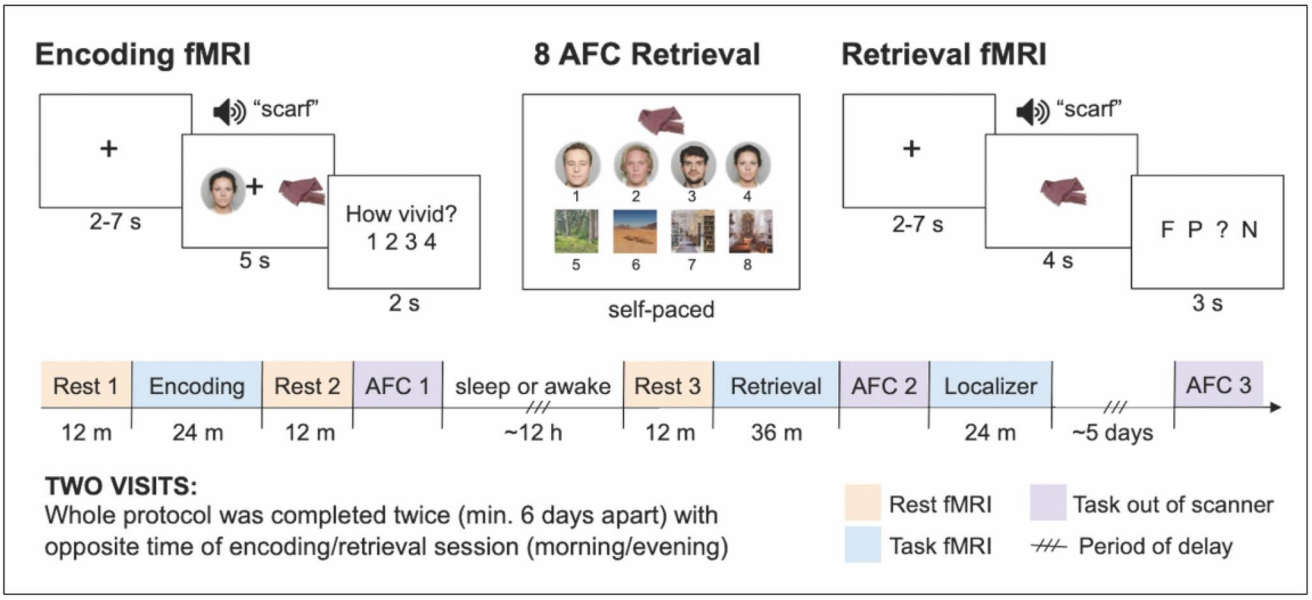

Fig. 1. Experiment structure. Participants completed a multimodal associative encoding task, visualizing interactions between items and face/place associates (concurrently, a voice named the item 3 times). Memory for the encoded associations was tested via offline forced-choice retrieval after 15 min, 12 h, and ~5 days, and during an in-scanner cued retrieval session taking place ~12 hours post-encoding. Here, a mix of previously encoded and novel items was presented, together with the items spoken name, and the participants indicated memory of the associate via F(ace) or P(place) responses, or alternatively item recognition without source information ("?") or no memory of seeing the item (N(ovel)). Resting-state fMRI series were acquired 3 times during the experiment: before encoding (baseline/pre-encoding), immediately following encoding ("post-encoding"), and immediately preceding in-scanner retrieval ("delayed post-encoding"). Functional localizer sessions were run at the end of the experiment. When possible, participants completed the entire experimental protocol twice (at least 6 days apart). The 2 visits differed only in time of encoding session (morning/evening) and consequently time of in-scanner retrieval, which occurred 12 h post-encoding. Eighty-three participants completed 2 full visits.

participants were instructed to stay awake, i.e. avoid naps, before in-scanner retrieval 12 h later. For the evening encoding session, the 12-h delay involved sleep at a hospital hotel associated with the scanner facilities. Order of visits was counterbalanced over participants.

Participants were thoroughly trained on the different task components before the experiment began and were informed that their memory for the encoded associations would be tested. All employees administrating the tasks were carefully trained to give identical task instructions across participants.

Experimental tasks and stimuli

Stimulus material (from both visits combined) consisted of a total of 384 real-life images of inanimate everyday items, 8 images of faces (4 males, 4 females), and 8 images of places (4 indoor, 4 outdoor), as well as 384 auditory stimuli in the form of a prerecorded (female voice) name for each item. All item/auditory stimuli were 2-syllable Norwegian words. Place stimuli and face stimuli were luminance-matched. A total of 256 items were presented at encoding, of which a predetermined half constituted the task material for participants' first visit (item images and corresponding auditory item-names 1–128, face images 1–4, and place images 1–4), and the other half of the stimuli constituted the task material for participants' second visit (i.e. item images and corresponding auditory item-names 129–256, face images 5–8, and place images 5–8). The remaining 128 item stimuli were introduced as novel items during in-scanner retrieval. Apart from the specific images used, the tasks were identical across visits. Training task stimuli consisted of 16 cartoon images and item-names from the same stimuli categories (i.e. items, faces, and places). Item images were obtained mainly from the Bank of Standardized Stimuli (Brodeur et al. 2010), some from StickPNG.com and from Google Advanced Image Search under the license "labelled for reuse with modification." Face images were obtained from Oslo Face Database (described in Chelnokova et al. 2014). Tasks were designed and run using MATLAB 9.7.0 and Psychtoolbox-3 3.0.16.

One session of the rapid event-related encoding task consisted of 128 trials of an alternating item-face/item-place associative task, 64 of each condition. One hundred and twenty-eight unique items were presented one at a time on the screen for 5 s together with either 1 of 4 real-life faces or 1 of 4 real-life places (16 trials per unique face/place). Concurrently with the visually presented stimuli, a female voice named the item 3 times (e.g. "scarf," "scarf," "scarf"). Participants were instructed to visualize an interaction between the item and the face or place associate before rating the vividness of the imagined interaction on a scale from 1 to 4 during a 2-s interval following stimulus offset. Finally, a fixation cross appeared and remained on the screen until the beginning of the next trial. Order of conditions and intertrial interval (ITI; 2–7 s) was optimized with optseq2 (http://surfer.nmr.mgh.harvard.edu/optseq/). Item-associate combinations were randomized over participants.

The offline memory test was an 8-alternative forced choice (AFC) test where all the items from the preceding encoding task were presented, one at a time, and the participants had to indicate which of the 8 possible associates (4 faces + 4 places) they thought the item was paired with at encoding, all in a self-paced manner. This test was performed immediately after post-encoding rest and also after ~12 h and ~5 days.

At in-scanner retrieval, a trial started with the presentation of a visual item and its spoken name (e.g. "scarf"). After a 5-s stimulus presentation period, a 2-s interval followed in which participants were asked to indicate their recollection of source information associated with the specific item. The 4 alternatives were as follows: (i) the item was presented together with a face stimulus

at encoding; (ii) together with a place stimulus at encoding; (iii) they remembered seeing the item at encoding but could not recall the associate; (iii) the item was not presented at encoding. One session of the retrieval task consisted of 192 trials of which 64 involved an encoding item presented with a face associate, 64 involved an encoding item presented with a place associate, and 64 involved a novel item (i.e. not presented at encoding). Fixation ITI varied between 2 and 7 s and was optimized with optseq2. Item presentation order was randomized over participants with the criterion that an equal number of face-encoded, place-encoded, and novel items were presented within a scanner run (3 runs in total per session).

The localizer task followed an ABN block design (Maus et al. 2010) in which two 12-s stimulus blocks were followed by a 12-s fixation block. A stimulus block consisted of continuous presentation of 1 out of 4 stimulus categories: faces from the encoding task, places from the encoding task, novel items, and scrambled versions of the novel items. During the face and place blocks, one specific face/place stimulus was held static on the screen and participants responded to miniature random changes to the image. During the item/scrambled items, block category stimuli were replaced every 1 s. Presentation order of stimulus blocks was optimized via custom routines that ensured (i) the same stimulus category was never presented 2 blocks in a row; (ii) over the full session, a specific face/place stimulus was preceded by all place/face stimuli; (iii) temporal distance between stimulus categories was held as short as possible. Each specific face/place stimuli, as well as the item/scrambled item categories, were presented 8 times over the 4 runs constituting a localizer session.

During resting-state recordings, participants were instructed to remain awake, keep eyes open, and focus on a fixation cross. Afterwards, participants completed a questionnaire of what they were thinking about during scanning.

MRI acquisition

Imaging data were collected with a 3T Siemens Prisma MRI unit equipped with a 32-channel Siemens head coil (Siemens Medical Solutions Germany) at Rikshospitalet, Oslo University Hospital, Norway.

Scanning parameters were equal across all fMRI experiments. Fifty-six transversely oriented slices were measured with a blood oxygen level-dependent (BOLD)-sensitive T2∗-weighted echo planar imaging sequence (time repetition [TR] = 1,000 ms; time echo [TE] = 30 ms; flip angle = 63°; matrix = 90 × 90; voxel size = 2.5 × 2.5 × 2.5 mm^3; field of view [FOV] = 225 × 225 mm^2; ascending interleaved acquisition; multiband factor = 4; phase encoding direction = AP). Each encoding, retrieval, and resting-state run produced 730 volumes while a localizer run produced 366 volumes. To allow for signal stabilization and avoid T1 saturation effects, the 6 first volumes of each fMRI run were discarded from the analyses, in addition to the volumes automatically discarded by the Siemens system. Sufficient T1 attenuation was confirmed following preprocessing.

Additional scans included spin-echo field map sequences with opposing phase-encoding directions acquired for distortion correction of the fMRI data; a T1-weighted MPRAGE sequence consisting of 208 sagittally oriented slices (TR = 2,400 ms; TE = 2.22 ms; TI = 1,000 ms; flip angle = 8°; matrix = 300 × 320 × 208; voxel size = 0.8 × 0.8 × 0.8 mm^3; FOV = 240 × 256 mm); a T2-weighted SPACE sequence consisting of 320 sagittally oriented slices (TR = 3,200 ms; TE = 5.63 ms; matrix = 320 × 300 × 208; voxel size = 0.8 × 0.8 × 0.8 mm^3; FOV = 256 mm × 240 mm). Additionally, a clinical T2w fluid-attenuated inversion recovery sequence was run and inspected by a clinical radiologist.

For the fMRI sequences, a NordicNeuroLab (NNL; NordicNeuroLab, Norway) 32-inch LCD monitor was positioned behind the scanner and viewed via a mirror attached to the head coil. Participants produced manual responses using a double, 2-button NNL ResponseGrip system. Auditory stimuli were presented to the participants with the OptoActive noise canceling (ANC) II headphones (Optoacoustics, Israel).

Preprocessing

We here followed lab routines that have been described in full in Ness et al. (2021). Briefly, we used the Nipype-based (Gorgolewski et al. 2011) FMRIPREP pipeline (version 1.5.3; Esteban et al. 2019), with a custom implementation (https://github.com/markushs/sdcflows/tree/topup_mod) of TOPUP distortion correction (Andersson et al. 2003). Quality control of raw+preprocessed data was performed via inspection of visual reports generated by FMRIPREP and MRIQC (Esteban et al. 2017). fMRI data were denoised prior to statistical analysis: Following nonaggressive removal of ICA AROMA-classified noise components (Pruim et al. 2015), average white matter and cerebrospinal fluid (CSF) signal timeseries (one-voxel 3D eroded masks of Freesurfer's individually segmented cerebral white matter and ventricular regions of interest (ROIs); parameters "–ctx-wm" and "–ventricles" in *mri_binarize*, respectively) were extracted from the AROMA-denoised data. Next, using Nilearn routines (nilearn.image.clean_img(); Abraham et al. 2014), data were detrended before temporal filtering and regression of WM and CSF timeseries from the AROMA-denoised data, ensuring orthogonality between filters and confound timeseries (Lindquist et al. 2019). Detrending in Nilearn works similar to scipy.signal.detrend() and involves subtraction of a linear least-squares fit from data. As Nilearn's clean_img-routines produce mean-centered timeseries, the mean voxel signal was added back to the denoised data to facilitate inspection. Localizer fMRI data were high-pass filtered at 0.005 Hz; encoding and retrieval fMRI data were high-pass filtered at 0.008 Hz (filter frequency based on slowest task fluctuation observed in the specific task paradigm). Resting-state data were bandpass-filtered between 0.008 and 0.09 Hz. Spatial smoothing (4 mm FWHM) was performed using Freesurfer routines for analyses performed at the surface level (localizer data). No smoothing was applied to data used for ROI/parcel-level analyses.

ROI definitions

Functional task-related ROIs were defined individually for each participant based on all available localizer runs from all visits to enable localization of brain areas thought to be especially relevant to the task stimuli in our task, namely face-sensitive fusiform face area (FFA), place-sensitive parahippocampal place area (PPA), and item-sensitive lateral occipital complex (LOC). A general linear model (GLM) was set up for each participant: the 4 stimulus categories (faces, places, items, and scrambled items) were modeled as blocks of 12 s duration according to their presentation schedule while task responses were modeled as stick events. The 5 task event descriptors were convolved with a canonical (two-gamma) hemodynamic response function (HRF) and added as regressors to the GLM together with their time and dispersion derivatives. Freesurfer FSFAST routines (https://surfer.nmr.mgh.harvard.edu/fswiki/FsFast) were used to estimate parameter estimates and their contrasts from surface level data in fsaverage5 space (10,242 vertices per hemisphere).

FFA was defined by surface vertices responding stronger to faces than places within the right posterior and mid fusiform gyrus (Kanwisher et al. 1997), PPA defined as vertices responding stronger to places than faces within the right parahippocampal gyrus (Epstein and Kanwisher 1998), and LOC as vertices responding stronger to items than scrambled items within the right lateral occipital cortex (Grill-Spector et al. 2001), all with an uncorrected threshold of $P < 0.0001$. If the number of remaining vertices was less than 5, the threshold was lowered until 5 or more contiguous significant vertices were observed. Seven participants had fewer than 5 LOC vertices at the initial P-threshold. Analyses containing LOC were run with and without these.

The hippocampus and subcortical control ROIs were derived from the Freesurfer automatic subcortical segmentation (Fischl et al. 2002). The selected control regions included thalamus (excluding lateral and medial geniculate bodies), caudate nucleus, putamen, and amygdala. All subcortical ROIs were bilateral. Caudate and putamen were selected based on observations of modulated functional connectivity in aging and during episodic memory operations involving these structures (Fjell et al. 2016; Ness et al. 2021). Amygdala was included as the structure lies adjacent to hippocampus and shares similar MRI signal-to-noise properties (Olman et al. 2009). Thalamus was included due to suggestions of it having a complementary role to hippocampus during consolidation states (Logothetis et al. 2012; Yang et al. 2019). All whole-brain parcel-level analyses were based on the Schaefer-Yeo 400 node cortical parcellation (Schaefer et al. 2018). Cortical network analyses were based on the Yeo 7-network resting-state parcellation (Thomas Yeo et al. 2011). All neocortical parcels/networks were established in participant space through intersections with the Freesurfer-derived cortical ribbon.

Supplementary analyses involved dividing the bilateral hippocampal ROI into anterior and posterior parts, using the uncal apex as reference (Poppenk et al. 2013). See Supplementary Fig. 1 and its caption for detailed description about the approach.

Preparations for statistical analyses

For preparation of data, statistical analyses, and visualization, we used Python 3.7.4, including the use of the packages Scikit-learn (version 0.23.2; Pedregosa et al. 2011), Nilearn (version 0.7.1; Abraham et al. 2014), and Pingouin (version 0.3.12; Vallat 2018). Linear mixed models were run in R 4.0.0 (R Core Team, 2022) via packages Lme4 (Bates et al. 2015) and Lmer4Test (Kuznetsova et al. 2017).

The following approach was used to extract rsfMRI BOLD timeseries and estimate functional connectivity measures for a given participant: (i) For the functionally defined ROIs (FFA, PPA, LOC), we ran principal component analysis (PCA) on vertex timeseries from a given ROI to account for the differences in ROI sizes across participants. The timeseries derived from the first PCA component was used as a representative measure of ongoing resting-state fluctuations within the ROI. (ii) For the anatomically defined subcortical ROIs, mean timeseries over functional voxels overlapping >50% with the high-resolution structural definition were extracted and averaged over hemispheres. (iii) For the whole-brain neocortical 400-node parcellation, functional voxels overlapping >50% with a given neocortical parcel, defined in native high-resolution structural space and constrained by the cortical ribbon, were considered functional representatives for that parcel and the associated timeseries were averaged. (iv) Measures of functional connectivity between timeseries were estimated by pairwise Pearson's correlation for each rest scan separately. The correlation coefficients were Fisher transformed to z-values and post-encoding modulation values were established by subtracting pre-encoding values from post-encoding values, separately for the immediate and 12 h delayed post-encoding rest periods for each visit. (v) Network level measures of functional connectivity change were established by averaging modulation values over all hippocampal edges (or other subcortical seed ROI in the control analyses) with neocortical parcels assigned to a given network (parcel-network correspondence obtained from https://github.com/ThomasYeoLab/CBIG/tree/master/stable_projects/brain_parcellation/Schaefer2018_LocalGlobal).

Task-specific functional connectivity during in-scanner encoding and retrieval was established using generalized psychophysiological interactions (gPPIs; McLaren et al. 2012). For the encoding data, 3 "psychological" timeseries were set up as boxcar functions, reflecting encoding events (5 s duration) characterized by "successful source memory encoding" or "unsuccessful source memory encoding", as well as response events (2 s duration). Memory status was derived from the offline 8AFC test occurring immediately following the post-encoding resting-state scan. For the retrieval data, 4 psychological timeseries were set up in a similar fashion reflecting "successful source memory retrieval," "misses" (old items not recognized with correct source information), novel items, and response events. Here, memory status was based on the in-scanner responses. Next, denoised task-state BOLD timeseries from hippocampus and 400 neocortical parcels were deconvolved into neuronal estimates (Gitelman et al. 2003) and point-by-point multiplied with the demeaned psychological event timeseries (Di et al. 2017). The resulting "psychophysiological" timeseries, one per event type, were returned to the BOLD level through convolution with a canonical 2-gamma HRF and included in GLMs together with HRF-convolved versions of the psychological functions and the original seed timeseries. As the current investigation focused on hippocampal–neocortical interactions, a total of 800 PPI GLMs was set up for each participant and task state. Four hundred of these used a neocortical node as source of the physiological signal in the design matrix and the hippocampal BOLD timeseries as dependent variable. The other 400 used hippocampus as physiological source in the design while the dependent variable spanned all neocortical nodes. Each neocortical node was thus represented on the dependent side in one model and the independent side in another. For our measure of nondirectional memory-relevant functional connectivity between hippocampus and a given neocortical node, we used the average of the parameter estimates associated with the PPI regressor representing successful memory trials in the 2 models including that node. Four hundred such symmetrized PPI measures (Di and Biswal 2019) representing the full hippocampal–neocortical modulation during source memory operations were established for both encoding and retrieval state data.

As the experimental paradigm consisted of separate independent memory tests of the encoded content—performed at different delay intervals—we established measures of task-relevant memory performance over 4 operationalizations: (i) immediate memory—proportion correct item-source assignments on the 8AFC test following immediately after the encoding scan; (ii) intermediate memory—proportion correct on the second AFC test ~12 h post-encoding, not including items with wrong source assignment at the immediate test; (iii) durable memory—proportion correct on the third AFC test ~5 days post-encoding, not including items with wrong source assignments in any of the earlier tests; (iv) category-level memory—proportion correct face/place assignments out of total exposures to encoded items

during in-scanner retrieval, corrected for wrong assignments (e.g. "face" response to item shown with place-associate).

Statistical analyses

Linear mixed models were used to test for post-encoding changes in rsFC between hippocampus and the localizer-derived category-sensitive ROIs (Fig. 2B) and between hippocampus and the 7 cortical networks (Fig. 4A). Here, post-pre difference in rsFC was fitted as a function of hippocampal ROI pair (alternatively network pair) and age group. As most participants went through the full paradigm twice, participant ID was added as random intercepts to account for multiple sessions. No global intercept was included in the model, allowing us to assess individual change for each ROI pair. Estimates of participant motion (mean framewise displacement [FD] over resting-state runs) and time of day (morning or evening scan) were added as covariates. FD, time of day, and age group were demeaned. *P*-values were adjusted for multiple comparisons using false discovery rate (FDR) correction (Benjamini and Hochberg 1995). The same modeling approach was used in control analyses with alternative subcortical ROIs (e.g. Fig. 4B). Additionally, to potentially observe if the post-encoding effects could be driven by the first few minutes following the previous encoding period, the same method was applied separately on the 6 first and the 6 last minutes of the immediate post-encoding rest period. Moreover, we directly tested whether there were differences in the values of rsFC changes between the first and the second half of the rest period with a one-sample *T*-test of the mean subtraction scores.

For the whole-brain parcel-wise analyses (Fig. 3A), we ran 400 linear regressions with hippocampal-parcel rsFC change as dependent variable and demeaned FD as covariate. Average functional connectivity change over 2 visits was used as dependent measure for participants who had been through both morning and evening scans ($N = 69$). In the remaining participants, i.e. those who had only one valid visit (see Section 2.2), morning and evening scans were equally distributed ($N = 20$; 10 morning scans, 10 evening scans). *P*-values derived from *T*-values of the intercepts were FDR-corrected for multiple comparisons and used to assess significance of rsFC change over hippocampal edges. The same approach was used in control analyses with alternative subcortical seed regions and in the parcel-wise analyses contrasting change in hippocampal–neocortical rsFC with similar measures derived from other subcortical ROIs (Fig. 3B). Observing no significant effects of individual motion on the rsFC change measures, seed-parcel rsFC change differences between age groups were tested using independent samples Welch separate variances *T*-test.

Nodal strength centrality differences were calculated from the individual subjects' weighted 405 × 405 neocortical + subcortical rsFC change graphs. A given node's strength was calculated as the sum of the weights of all edges connected to that node (Fornito et al. 2016). For visualization (Fig. 3C), the strength values were averaged across participants and sorted into constituent canonical resting-state networks. Paired *T*-tests were used to assess differences between hippocampal post-pre strength change and strength changes observed in all other nodes (404 tests in total). Significance was established after FDR adjustment of *P*-values.

The comparisons of hippocampal–neocortical post-encoding rsFC change patterns with task-derived gPPI patterns of hippocampal functional connectivity during source memory encoding and retrieval operations (Fig. 5) were performed using rank-based (spearman) spatial correlations. Empirical spatial correlations between rsFC change and gPPI patterns were compared to null distributions of 1,000 similar spearman correlations, but where the rsFC change pattern had been permuted spatially. This was performed both without considering spatial autocorrelations in the data (i.e. via numpy.random.permutation), or via BrainSMASH (Burt et al. 2020) to ensure similar overall spatial autocorrelation structure in the permuted rsFC data as in the original rsFC data. Spatial autocorrelation structure was estimated at the surface level, for each hemisphere separately, after calculating geodesic distance between the 200 parcels in a hemisphere using the Python package surfdist (Margulies et al. 2016).

Global signal timeseries, to be used in control analyses, were extracted from all participants' baseline rsfMRI scans using a Freesurfer-derived gray matter mask and AROMA-denoised data. For each participant, Spearman correlations between the global signal and BOLD-timeseries from subcortical ROIs during the same baseline scan were estimated and Fisher-transformed before being averaged across visits. Group-level differences between subcortical structures' baseline correlation with the global signal were tested using paired-samples *T*-tests.

Associations between individual differences in memory performance and post-encoding hippocampal rsFC modulations were tested over 4 operationalization of retention success, using linear mixed models at the category-selective ROI level and network level, and partial Spearman correlations at the whole-brain parcel level. A linear mixed model was run for each hippocampal ROI pair (alternatively network pair) separately; here, memory performance was fitted as a function of rsFC change and age group, participant ID included as random intercepts to account for multiple visits, and time of day added as covariate. The partial correlations were run iteratively over hippocampal rsFC change with the 400 neocortical parcels, including participant age as covariate. We also estimated rsFC change within a mask consisting of the 305 nodes showing increased post-encoding rsFC with the hippocampus (i.e. one value per participant) and compared this "global" hippocampal–neocortical change measure with our memory performance measures using a similar partial correlation approach. In order to see if there were any biases in rsFC concerning stimulus-specific retention, we estimated a difference score per retention measure per participant reflecting memory bias towards face associations or place associations (i.e. source performance for faces minus source performance for places). We also estimated the per-participant difference score in hippocampal coupling with FFA and PPA from the post-encoding period (i.e. HC-FFA rsFC minus HC-PPA rsFC). Spearman correlation was applied for all 4 retention tests. All *P*-values were FDR-corrected for multiple comparisons. As a few participants missed data on some of the memory tests, the number of observations entered in the analysis varied slightly between operationalizations. Sample sizes for the different tests are reported in Table 2. All participants scored above chance level for all 3 AFC-based memory operationalizations (>12.5%, >1.56%, and >0.2%, respectively). When correcting correct trials with incorrect source trials for the in-scanner retrieval, all except one participant with score 0 had positive scores.

Data availability

Code required to reproduce results and figures presented in the current report will be made available at https://doi.org/10.5281/zenodo.5829424.

Results

Increase in rsFC between hippocampus and targeted stimulus-sensitive ROIs after encoding

To replicate previous reports of increased rsFC between hippocampus and task-related regions following extensive encoding

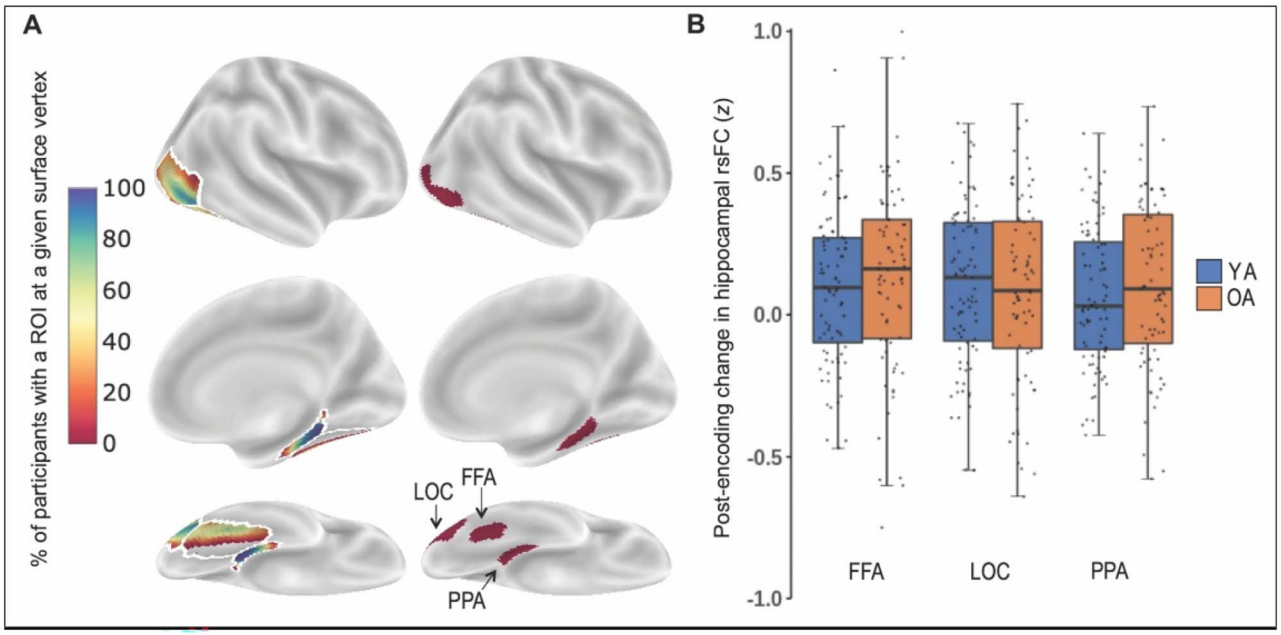

Fig. 2. A) Left part shows % of participants with a ROI at a given surface vertex within the anatomical masks (white outline). Right part shows example of category-sensitive regions, defined from the functional localizer protocol (lateral, medial, and inferior views of the right inflated hemisphere). B) Estimated post-pre change in hippocampal rsFC with the 3 ROIs, separated over age groups (YA/OA = younger/older adults). Boxplot whiskers represent the 1.5 interquartile range.

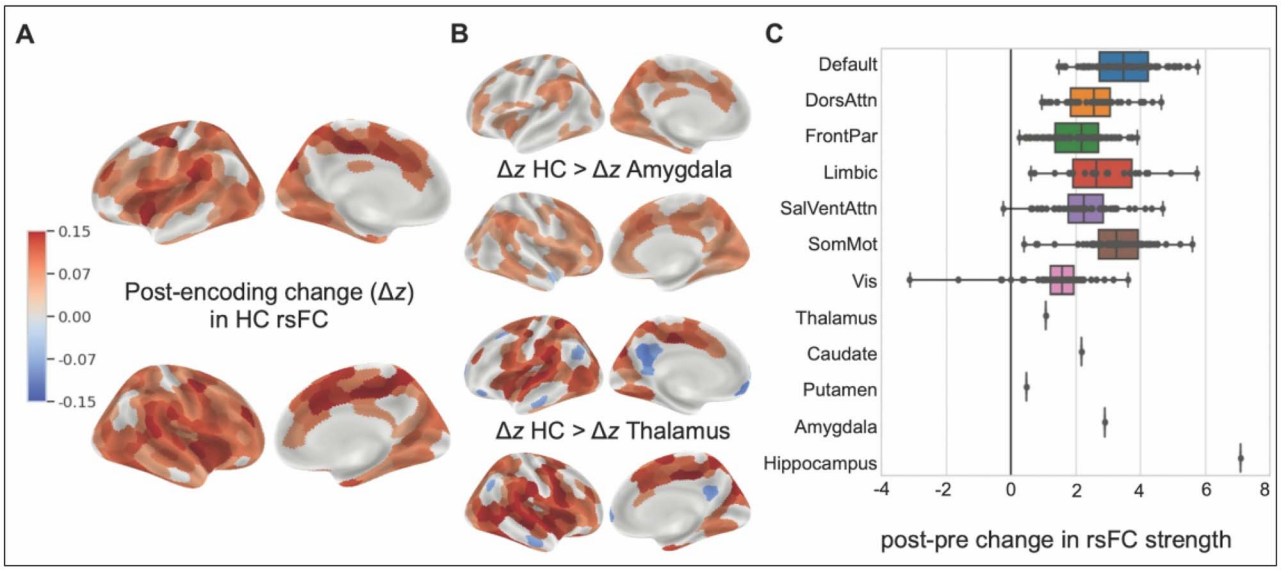

Fig. 3. A) 305 nodes showing significant FDR-corrected post-encoding change in rsFC with hippocampus (values represent difference in Fisher-transformed *r*). B) Nodes for which hippocampal rsFC change was significantly (FDR-corrected) different when controlling for change observed using alternative subcortical seed ROIs (amygdala and thalamus as examples, see Supplementary Fig. 3 for other control seeds). C) Post-pre rsFC centrality (strength) change per node. Each dot represents a node; neocortical nodes have been arranged into constituent resting-state networks. Boxplot whiskers represent min/max observed nodal value within a network, while box limits reflect quartiles; black vertical line represents median strength. SalVentAttn, saliency/ventral attention network; DorsAttn, dorsal attention network; Vis, visual network; FrontPar, frontoparietal network; SomMot, somatomotor network; default, default mode network.

tasks, we correlated BOLD time series extracted from hippocampus with those from stimulus-sensitive regions, individually defined from the functional localizer protocol (Fig. 2A). We then subtracted pre-encoding baseline correlations from post-encoding correlations. The resulting rsFC change measures, one per ROI-pair per participant, were assessed with a linear mixed model fitted as a function of ROI pair and age group. From the model conducted for hippocampus and the targeted stimulus-sensitive ROIs, FFA (sensitive to face stimuli), LOC (objects), and PPA (places/scenes), we observed a post-encoding increase in rsFC compared to baseline for all ROI pairs (FDR-corrected $P_{FDR} < 0.002$) with estimates (change in z-transformed *r*) ranging from 0.08 to 0.12 (Fig. 2B, Supplementary Table 1). No main effect of age was observed. Excluding 15 observations from 10 participants with LOC < 5 vertices did not change the results. Repeating the analyses over anterior and posterior hippocampus separately produced similar main effects (Supplementary Fig. 1). Alternative approaches for defining the localizer ROI did not change the

Table 2. Hippocampal rsFC and memory performance.

Memory performance operationalization	Immediate memory (~1 h, 8AFC)	Intermediate memory (12 h, 8AFC)	Durable memory (5 days, 8AFC)	Category-level memory (12 h, scanner)
YA performance	$N = 46$	$N = 46$	$N = 45$	$N = 47$
	74.0% (16.8)	64.1% (21.0)	52.8% (22.3)	70.1% (19.7)
OA performance	$N = 42$	$N = 42$	$N = 42$	$N = 42$
	54.6% (18.7)	39.5% (19.4)	28.8% (16.0)	48.8% (23.5)
Whole-brain (400 edges), Partial spearman (top rho shown)	0.35 (0.32)	0.29 (0.26)	−0.32 (−0.30)	−0.30 (−0.29)
	all $P_{FDR} > 0.05$	all $P_{FDR} > 0.05$	all $P_{FDR} > 0.05$	all $P_{FDR} > 0.05$
Yeo 7 networks, Linear mixed model (top estimate shown)	14.31	10.89	2.42	11.10
	all $P_{FDR} > 0.05$	all $P_{FDR} > 0.05$	all $P_{FDR} > 0.05$	all $P_{FDR} > 0.05$
	($P = 0.05$)	($P = 0.27$)	($P = 0.24$)	($P = 0.22$)
Localizer ROIs	2.82	1.19	−2.40	4.10
Linear mixed model (top estimate shown)	all $P_{FDR} > 0.05$	all $P_{FDR} > 0.05$	all $P_{FDR} > 0.05$	all $P_{FDR} > 0.05$
	($P = 0.51$)	($P = 0.81$)	($P = 0.61$)	($P = 0.35$)
Global mask	−0.02 (−0.12)	−0.03 (−0.11)	−0.06 (−0.17)	−0.03 (−0.12)
Partial spearman (rho reported)	$P = 0.85$ (0.28)	$P = 0.82$ (0.31)	$P = 0.58$ (0.12)	$P = 0.74$ (0.25)
Memory (Face – Place) vs. (HC-FFA – HC-PPA)	0.21 (0.22)	0.12 (0.13)	0.29 (0.29)	−0.06 (−0.03)
Partial spearman (rho reported)	$P = 0.05$ (0.04)	$P = 0.26$ (0.23)	$P = 0.007$ (0.007)	$P = 0.58$ (0.81)

Note: Results of tests of associations between individual differences in memory performance and post-encoding rsFC modulations. Performance columns (YA/OA = younger/older adults) show mean correct source memory with standard deviations in parenthesis. Partial correlation results columns (whole-brain, global mask, and FFA/PPA analysis) show results without (outside parenthesis) and with participant age (inside parenthesis) included as covariate. Linear mixed models results show lowest *P*-value observed in parenthesis.

results, including drawing a same-sized cluster around a peak voxel and when stripping this cluster for vertices responding stronger to the other 2 stimuli categories.

Widespread increase in hippocampal–neocortical rsFC after encoding

Next, to assess the extent of post-encoding changes in hippocampal–neocortical rsFC beyond stimulus-category sensitive cortex, we first ran a whole-brain analysis testing for post-pre modulation between the hippocampus and each of 400 nodes in a pre-established neocortical parcellation (Schaefer et al. 2018). Following FDR-correction, 305/400 nodes showed significant ($P_{FDR} < 0.05$) post-encoding increases in their rsFC with hippocampus (Fig. 3A), indicating that the observed increased coupling with stimulus-sensitive regions occurs as part of an extensive post-encoding modulation of hippocampal functional connectivity, affecting large portions of the cerebral cortex. No differences were found between the anterior and posterior hippocampus in this pattern of neocortical modulation (Supplementary Fig. 1).

To test whether the magnitude of this nearly global increase in post-encoding rsFC was specific to the hippocampus, we first repeated the analysis after subtracting post-pre rsFC changes between alternative subcortical seed ROIs and the same 400 neocortical nodes (Fig. 3B). Most of the observed changes remained significant ($P_{FDR} < 0.05$) after controlling for post-pre rsFC modulations using the following control seed regions: amygdala (201/400 nodes still significant), caudate nucleus (213/400 nodes), putamen (276/400 nodes), and thalamus (237/400 nodes). The specificity of hippocampus' post-encoding behavior was further tested by calculating change in the graph-theoretical centrality measure "strength"—the sum of a node's edges in a weighted graph—for all neocortical and subcortical nodes: here hippocampus showed a numerically larger increase than any other node (Fig. 3C). Direct comparisons confirmed that hippocampus' change in strength was significantly larger than that observed for 391 out of the 404 remaining nodes (including 4 subcortical) in the graph ($P_{FDR} < 0.05$). That is, using rsFC strength as a proxy for centrality in the full brain network, hippocampus showed higher post-pre centrality increase than most other nodes in the brain. Interestingly, the few remaining neocortical nodes *not* significantly different from hippocampus in terms of post-pre change in rsFC strength were mainly located along the (ventro)medial surface of prefrontal cortex. While it is beyond the scope of the current paper to investigate all post-encoding dynamics in detail, we include a short presentation and discussion of those nodes in Supplementary Fig. 2 and its caption.

The nearly global changes in hippocampal rsFC strength following our encoding task were also observed at the network level. A linear mixed model assessing change in rsFC between hippocampus and 7 cortical networks (Thomas Yeo et al. 2011) showed rsFC increases with all networks (all $P_{FDR} < 0.05$; Fig. 4A, Supplementary Table 2). Highest estimates of rsFC change were seen for the ventral and dorsal attention network while the lowest estimate was associated with the default mode network (DMN). No main effect of age was observed. Among the subcortical control regions, only amygdala showed significant post-encoding rsFC changes at the network level, with dorsal and ventral attention networks and the somatomotor network ($P_{FDR} < 0.02$; Fig. 4B).

Post-encoding change in hippocampal rsFC not present after 12 h

We next tested the duration of the observed changes in post-encoding hippocampal–neocortical rsFC. We calculated a second rsFC change measure, this time subtracting pre-encoding baseline correlations from hippocampal–neocortical correlations established using resting-state data collected ~12 h post-encoding. As participants were scanned over 2 visits, with baseline resting-state scans once in the morning and once in the evening (and similar for the 12 h delayed resting-state scans; see Fig. 1), we avoided potential time-of-day effects by averaging change measures from the 2 visits. Following the same approach as for the original rsFC change analysis reported above, we observed no significant change in hippocampal rsFC; not at the single parcel level, nor at the network or stimulus-sensitive ROI level. Moreover, the observed hippocampal rsFC change from baseline to immediate post-encoding rest was significantly greater than the (nonsignificant) change observed over 12 h (paired *T*-test of values extracted from the "global" hippocampal rsFC change mask: $t(168.5) = 2.48$,

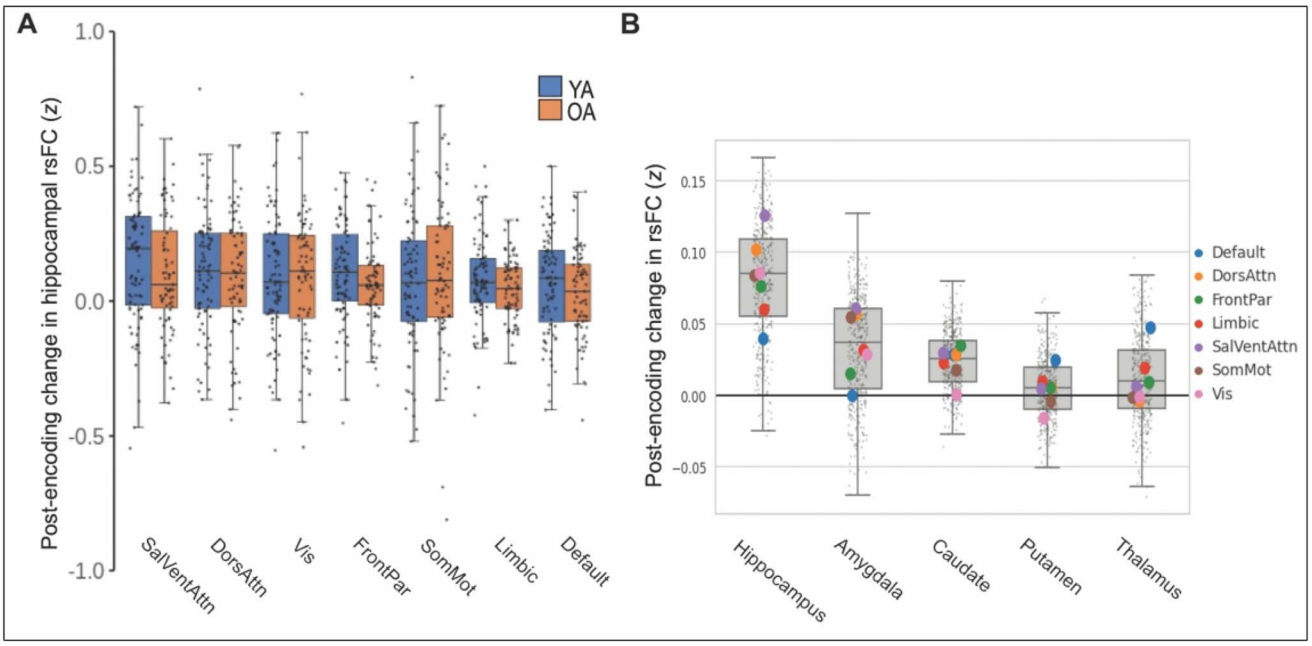

Fig. 4. A) Estimated hippocampal rsFC change with 7 neocortical networks, separated over age groups. Boxplot whiskers represent the 1.5 interquartile range. B) Subcortical seed ROIs change in rsFC with 400 neocortical nodes (gray dots) and networks (colored circles). Box plot whiskers represent ±1.5 interquartile range, while box limits reflect quartiles; gray horizontal lines show median changes in z. SalVentAttn, saliency/ventral attention network; DorsAttn, dorsal attention network; Vis, visual network; FrontPar, frontoparietal network; SomMot, somatomotor network; default, default mode network.

$P = 0.014$; 192/400 edges with $P_{FDR} < 0.05$ when tested independently, Supplementary Fig. 4). The extensive post-encoding hippocampal rsFC modulations thus appear to be transient in nature, increasing immediately following an intensive learning experience but returning to baseline levels within a 12-h timeframe.

Increases in hippocampal–neocortical rsFC not explained by global signal

To ensure that the nearly global upregulation of hippocampal functional connectivity post-encoding was not driven by residual noise in our data, we compared all subcortical seeds' baseline (i.e. pre-encoding) correlation against the global gray matter signal. The globally averaged signal (GS) is often considered a measure of spatially diffuse hemodynamic fluctuations of partly non-neuronal origin, understood as noise in the current context (Tong et al. 2019). If hippocampal dynamics mimic these non-neuronal contributors disproportionally, and the noise contribution to the hippocampal signal increases from pre- to post-encoding, this could theoretically result in apparent and increased coupling between HC and gray matter globally—and more so than for less noise-prone regions. Several of the other subcortical seeds, however, showed significantly stronger baseline correlations with the GS than hippocampus (mean $r = 0.36$), including both the thalamus (mean $r = 0.52$; paired T-test; $t(88) = 7.32$; $P < 0.001$) and caudate nucleus (mean $r = 0.44$, $t(88) = 7.00$; $P < 0.001$). As none of these nodes showed similar post-encoding rsFC changes as the hippocampus, associations with the global signal cannot explain the current results.

Post-encoding modulation of hippocampal rsFC mimics encoding patterns

To further characterize the hippocampal–neocortical rsFC change patterns, we compared the spatial profile of modulation observed during post-encoding rest with profiles estimated from encoding and retrieval task periods. Using gPPI analysis (McLaren et al. 2012; Di and Biswal 2019), we established spatial maps of average hippocampal modulation during the 2 task states (Fig. 5A). The specific contrasts used reflected changes in hippocampal functional connectivity during successful source memory operations, controlling for intrinsic connectivity between nodes, and correlated stimulus-induced activation effects. Spatial Spearman correlations between the post-encoding resting-state pattern and gPPI effects observed during active encoding revealed significant similarities in hippocampal–neocortical modulations across the states (rho = 0.427; $P < 0.001$; Fig. 5B). A positive relationship was also found with the retrieval-state gPPI pattern (rho = 0.207; $P < 0.001$), albeit significantly weaker than the spatial correlation observed with encoding data ($z = 3.47$; $P = 0.0005$). Additional analyses comparing the observed relationships with permuted null distributions preserving the spatial autocorrelation structure of the empirical brain maps confirmed significant similarities between encoding-state and post-encoding rsFC modulations (left hemisphere rho = 0.36, $P = 0.014$; right hemisphere rho = 0.54, $P < 0.001$; Fig. 5C). The retrieval-state gPPI pattern did however not share significant similarities with the post-encoding rsFC change map when controlling for spatial autocorrelations in the data (left hemisphere rho = 0.15, $P = 0.31$; right hemisphere rho = 0.23, $P = 0.10$). Thus, global post-encoding changes in hippocampus' functional connectivity profile preferentially resemble the effect of active encoding.

In order to unveil if effects during post-encoding rest were driven only by the first few minutes of the post-encoding rest period, we split the post-encoding rest period into 2 halves and analyzed them separately. Both the first and the second half of the immediate post-encoding rest period (6 min each) showed the same widespread pattern of hippocampal rsFC upregulation as reported earlier, except there was no significant change in HC-DMN for the first half ($P = 0.07$). The mean subtraction values

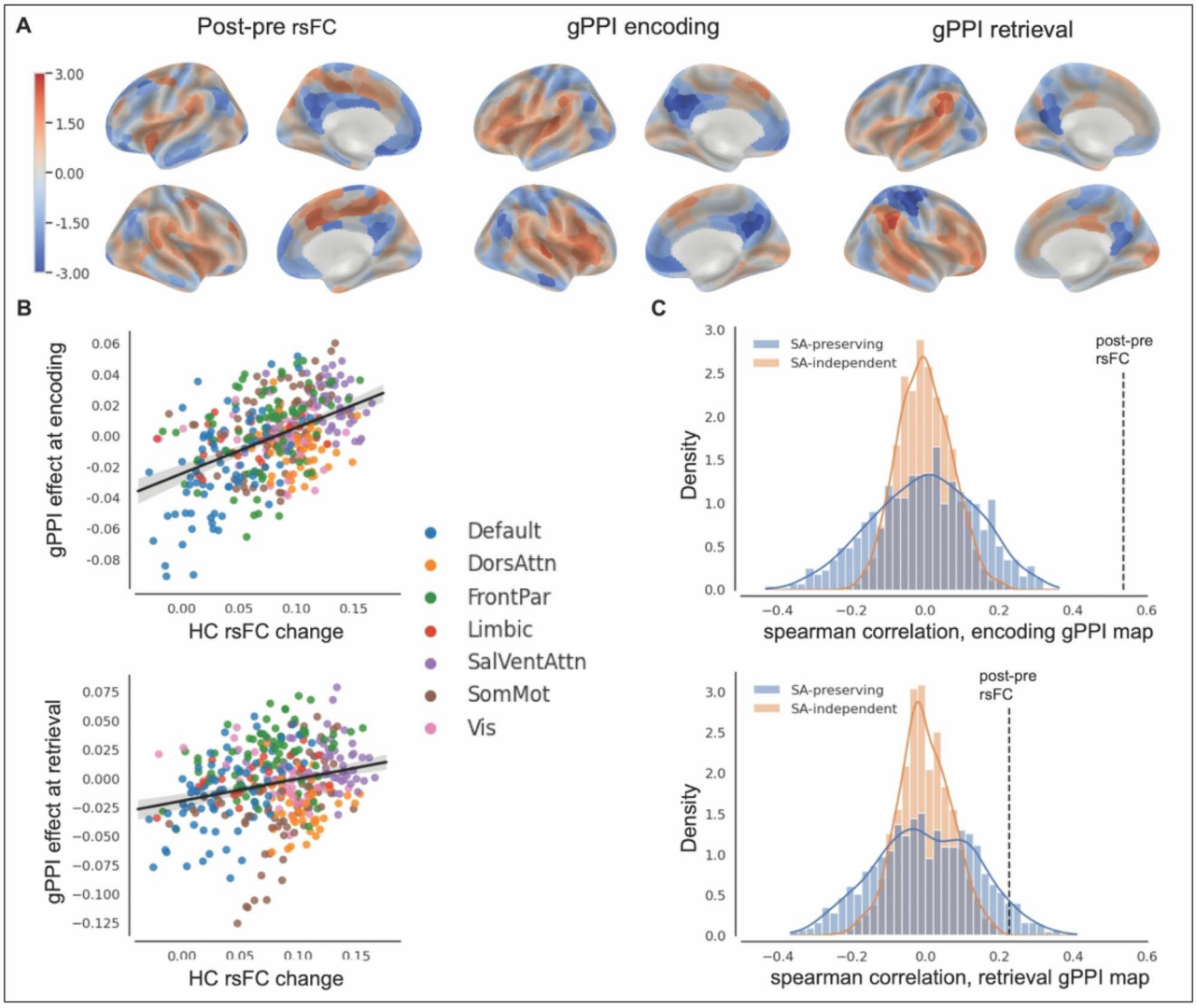

Fig. 5. A) Z-standardized maps of average hippocampal functional connectivity changes during resting and task states. B) Scatterplots showing relationships between task-state encoding (top) and retrieval (bottom) modulations and post-pre rsFC change in hippocampal (HC) functional connectivity with 400 neocortical nodes. Network membership of a node is indicated by its color. SalVentAttn, saliency/ventral attention network; DorsAttn, dorsal attention network; Vis, visual network; FrontPar, Frontoparietal network; SomMot, Somatomotor network; default, default mode Network. C) Permuted null distributions of spearman correlations between brain maps either ignoring (SA-independent) or incorporating (SA-preserving) spatial autocorrelation (SA) structures in the data. Dashed vertical lines show empirical correlation between the patterns. Results shown are from right-hemispheric data; similar results were observed in the left hemisphere.

between the halves were different from zero, in the direction of the second half (stimulus-sensitive ROIs: $t(88) = -2.05$, $P = 0.04$, network level: $t(88) = -2.71$, $P = 0.01$).

Post-encoding change in hippocampal rsFC is independent of age

Having established that post-encoding change in HC rsFC involves edges throughout the entire neocortex—in a pattern resembling memory encoding behavior—we tested whether this nearly global modulation was influenced by age. Participant age did however not explain significant variance in the observed reactivation-like connectivity profiles at any resolution or analysis level (category-selective ROI level: see Supplementary Table 1; network level: see Supplementary Table 2; neocortical parcel level: all $P_{FDR} > 0.05$). Similarly, we estimated average rsFC change within a mask consisting of the 305 nodes showing increased post-encoding rsFC with the hippocampus, i.e. one value per participant. Comparing this "global" hippocampal rsFC change measure between younger and older adults also did not reflect any age differences (Welch separate variances T-test; $t(86.99) = 0.76$, $P = 0.45$).

Post-encoding change in hippocampal rsFC and memory performance

Individual differences in episodic memory performance were not directly associated with our measures of hippocampal post-encoding modulation. This was true over a range of tests spanning retention intervals of hours to several days and involving both cued retrieval and forced-choice tasks (Table 2). However, we found a significant correlation between durable memory (~5 days) and hippocampal rsFC when we corrected for biases in retention of faces/places and correlated this with the difference in hippocampal coupling with FFA and PPA from the post-encoding period (rho = 0.29, $P_{FDR} = 0.028$).

Post-encoding default mode network modulations via thalamic interactions

The focus of the current study concerned reactivation-like modulations in hippocampal rsFC. However, considering recent reports of temporal co-occurrence of neurophysiological measures of hippocampal replay and activity increases in the DMN (Kaplan et al. 2016; Higgins et al. 2021), an observation from our control analyses warranted a post hoc investigation. In our data, hippocampus showed reliable coupling to the DMN both during pre- and post-encoding resting-state periods, i.e. when the periods were investigated in isolation (Fig. 6A). Yet, hippocampal post-pre rsFC change toward the DMN was the weakest observed at the network level (Fig. 4A). This was also reflected at the whole-brain parcel level. Here, hippocampus showed increased post-encoding coupling nearly globally across edges, with the conspicuous exception of a set of central DMN regions (medial prefrontal cortex, precuneus, angular gyrus; see Fig. 3A). Thalamus, one of the subcortical control seeds, did however show a clear post-encoding modulation of its rsFC with core DMN regions (Fig. 6). Moreover, for several DMN nodes, this change was significantly stronger than that observed for the hippocampus (see Fig. 3B). Interestingly, we found a significant positive relationship between the observed thalamic rsFC change pattern involving DMN nodes and the corresponding hippocampal–thalamic pattern across individuals (partial spearman correlation, with/without age as covariate: rho = 0.56/0.56; $P < 0.001$; Fig. 6C). This relationship remained significant when including observed rsFC change between hippocampus and the same DMN nodes as covariate, indicating unique shared variance between thalamus' links with DMN and the hippocampus (with-/without age as covariate: rho = 0.43/0.43; $P < 0.001$).

As participants showing strong rsFC change along edges linking thalamus and DMN also showed strong post-encoding thalamo-hippocampal modulation, we tested whether this relationship was reflected in hippocampus' post-encoding behavior toward the rest of the brain. That is: Does change in coupling between thalamus and DMN coincide with the observed changes in hippocampal rsFC to other neocortical nodes? A meditation analysis revealed a positive relationship between individual differences in thalamus–DMN coupling change (the average over thalamic edges seen in Fig. 6B) and mean post-encoding modulation over the "global" hippocampal–neocortical change pattern (as seen in Fig. 3A): P(Total Effect) = 0.019. This relationship was however fully mediated by the observed rsFC modulation in the hippocampus–thalamus link (bootstrapped P(Direct Effect) = 0.93; P(Indirect Effect) < 0.001; Fig. 6D). In other words, 2 independent networks, the hippocampal post-encoding modulation pattern and the corresponding DMN-centered thalamic pattern, covary in strength across subjects, and our results suggest this statistical relationship is mediated via interconnections between the 2 subcortical seed regions. Thus, while hippocampal interactions with the DMN do not, on average, change significantly following an intense encoding period, relationships observed through individual differences still suggest modulating influences between hippocampus and DMN via a thalamic pathway. These observations complement recent reports linking hippocampal replay with neocortical activity patterns (Higgins et al. 2021) and will be discussed in the following section.

Discussion

We here demonstrate continuation of a memory encoding state into task-free post-encoding rest. Following a period of intensive encoding, hippocampus increased its functional connectivity with large parts of the neocortex—over 75% following corrections for multiple comparisons at the current parcellation resolution. Although these modulations in hippocampal functional connectivity were measured during awake passive rest, their spatial profile across the neocortex resembled hippocampal connectivity patterns observed during active encoding of multimodal stimuli. Importantly, the observed modulations involved regions outside of sensory/perceptual and stimulus-category sensitive cortex; in fact, all the brain's major functional networks showed some degree of change in their post-encoding hippocampal interactions when contrasted with a pre-encoding baseline. These observations were not associated with participant age.

Such imaging-derived encoding-state continuation into task-free periods has been interpreted as evidence for "reactivation" (Tambini and Davachi 2019)—potentially reflective of hippocampal–neocortical co-activation patterns seen during neural "replay" in awake resting animals (Logothetis et al. 2012; Kaplan et al. 2016), and recently in humans (Higgins et al. 2021). In line with the long tradition connecting hippocampal replay during sharp-wave ripples with memory consolidation processes (Buzsáki 2015; Foster 2017), post-encoding reactivation observed in human fMRI data has reliably been linked with non-declarative (de Voogd et al. 2016; Jacobacci et al. 2020; Buch et al. 2021) and declarative memory processes, the latter through associations with episodic memory performance or detections of stimulus-specific activation patterns (Tambini et al. 2010; Deuker et al. 2013; Staresina et al. 2013; Schlichting and Preston 2014; Gruber et al. 2016; Murty et al. 2017, 2019; Schapiro et al. 2018). With few exceptions, however (Kukolja et al. 2016; Tompary and Davachi 2017; Cowan et al. 2021), previous approaches investigating reactivation in human participants have been limited to interactions within the medial temporal lobe (MTL) or between hippocampus/MTL structures and a few selected ROIs. We here replicate observations of increased post-encoding hippocampal connectivity with face-, place-, and object-sensitive regions (e.g. Tambini et al. 2010) but also show that these modulations must be understood as part of a nearly global pattern of hippocampal coupling change.

Given the structural similarities between this extensive hippocampal post-encoding coupling change pattern and the global hippocampal–neocortical pattern extracted from the encoding state, we suggest that reactivation may not be limited to reinstatement of relevant sensory characteristics of the encoding task but also incorporate encoding-relevant processes typically associated with higher-order functional networks, such as attentional allocation, schema integration, and cognitive control (Kim 2011; Beason-Held et al. 2021). In line with this view, previous ROI-focused fMRI studies in humans have reported post-encoding modulations consistent with integration of novel information in resting-state interactions between hippocampus and ventromedial prefrontal cortical regions (van Kesteren et al. 2010; Schlichting and Preston 2016; Tompary and Davachi 2017). Moreover, studies in rhesus monkeys combining electrophysiological recordings and fMRI have found activity increases coinciding with hippocampal ripple events throughout higher-order cerebral cortex (Logothetis et al. 2012; Kaplan et al. 2016). Similarly, a recent MEG study in humans found activity increases source-localized to the parietal lobe ("parietal alpha network") and DMN regions during hippocampal ripple events detected during awake rest (Higgins et al. 2021). It should be noted, however, that such ripple-synchronized activity does not indicate causal or direct relationships/connectivity between the hippocampus and neocortical regions. For example, theoretical accounts (Aggleton et al. 2016)

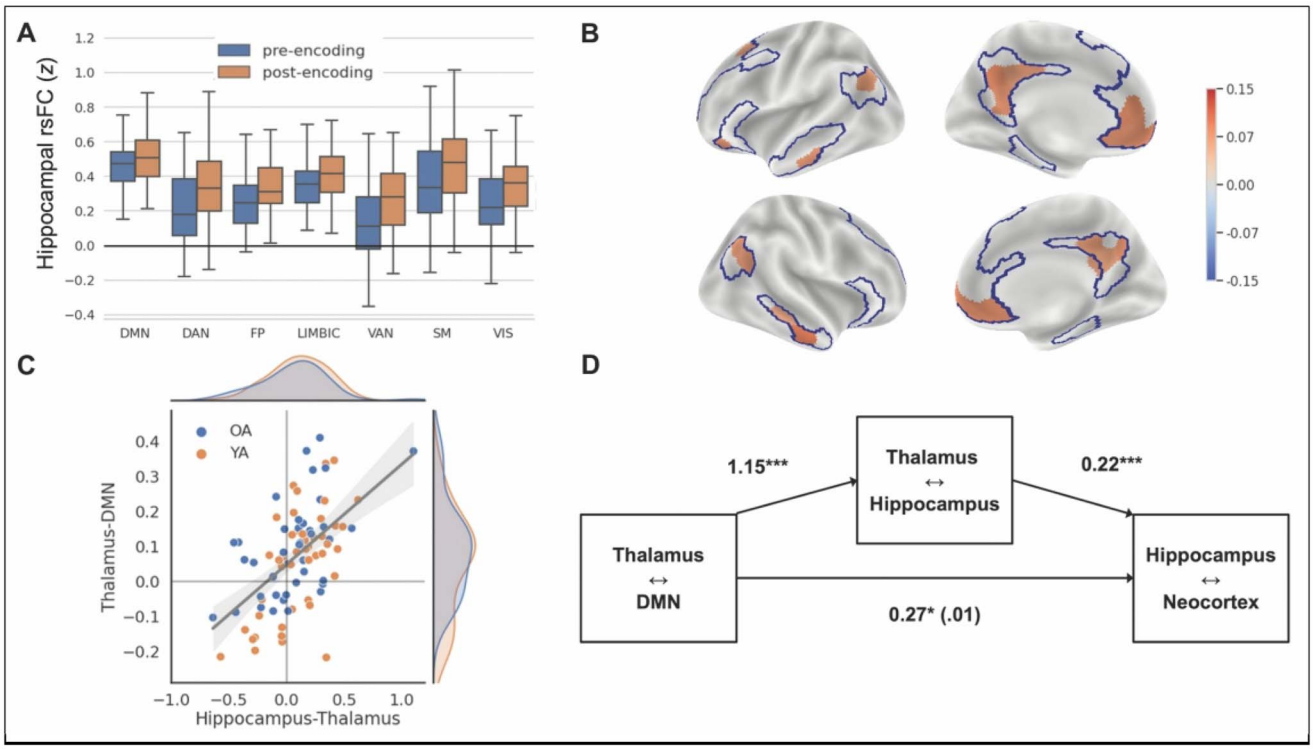

Fig. 6. A) Mean hippocampal rsFC over neocortical networks, estimated separately for pre-encoding and the post-encoding scans. DAN, dorsal attention network; FP, frontoparietal network; VAN, ventral attention network; SM, somatomotor network; VIS, visual perceptual network. Boxplot whiskers represent the 1.5 interquartile range. B) Nodes showing significant FDR-corrected post-encoding change in rsFC with the thalamus (values represent difference in Fisher-transformed *r*). DMN, derived from Yeo's 7-network parcellation outlined in blue. C) Relationship between hippocampal–thalamic post-pre rsFC change and average change over the thalamic edges shown in (B). OA, older adults; YA, younger adults. D) Schematic of mediation model. "Thalamus-DMN" equals the average over edges shown in (B). regression coefficient values from the model estimated with "hippocampus-neocortex" equaling the average over edges shown in Fig. 3A. Total effect coefficient presented outside parenthesis, direct effect presented inside. Two edges overlapping between the hippocampal and thalamic networks patterns were excluded from the calculations.

and fMRI investigations (Wagner et al. 2019) of post-encoding recruitment of the DMN report evidence for thalamic mediation of consolidation-related activity patterns. Our results provide further support for these accounts by the observation of robust functional post-encoding DMN-modulation through thalamic interactions but less so with the hippocampus as seed region. Moreover, we observed a covarying relationship between the hippocampal post-encoding modulation pattern and the corresponding DMN-centered thalamic pattern, fully mediated by the changes in the hippocampus-thalamus coupling.

While investigations of hippocampal interactions with other subcortical structures—e.g. the thalamus—appear promising in understanding the complex dynamics behind brain states supportive of ripple generation and memory reactivation (e.g. Yang et al. 2019), we found it noteworthy that the hippocampus showed the largest post-encoding change in its functional connectivity toward all other nodes in our parcellation, i.e. larger than any other subcortical or neocortical node. The fact that the upregulation of hippocampal coupling was absent when estimated from a second resting-state dataset collected ~12 h post-encoding supports the current view of hippocampus' unique role in the initial stabilization of memory traces (e.g. O'Neill et al. 2010) and resonates with animal studies showing high prevalence of hippocampal replay immediately after an experience, followed by a gradual decay in replay occurrences (Carr et al. 2011). When or how fast this decay appears in the form of rsFC modulations is currently uncertain.

Our reported measure of hippocampal functional connectivity change is however not a direct reflection of replay or replay-related processes as described in the neurophysiological literature. Although neuronal reactivation in principle can be detected at the BOLD response level (see Tambini and Davachi 2019 for a thorough discussion), without simultaneous neurophysiological measurements we cannot know what drives the observed increases in hippocampal coupling. We thus believe the transient centrality boost seen for hippocampus in the post-encoding functional brain network can be interpreted within the context of human imaging-based approaches to reactivation and consolidation processes. Here, post-encoding modulations of pairwise regional BOLD synchronicity have repeatedly been used to predict memory-relevant behavior and through this established a plausible mapping between the methodological approach and the underlying phenomenon of interest, memory consolidation (reviewed in Tambini and Davachi 2019). As we did not observe any direct associations with memory performance, we cannot draw a similar link between post-encoding functional connectivity and memory-relevant offline processing in our sample. When we corrected for biases in retention of faces/places, we found a significant correlation between durable memory (defined as memories lastingmore than 5 days) and hippocampal rsFC with FFA/PPA, respectively. This suggests some degree of task specificity in hippocampal rsFC in our data. The lack of direct, uncorrected correlations between hippocampal coupling and memory performance can have a

number of reasons and implications. Most importantly, this suggests that the nature of the process is perhaps not as straightforward as shown earlier. By using a link to memory performance to make inferences about the underlying cognitive processes, we are using between-subject differences to make inferences about within-subject processes, which is challenging. A correlation between rsFC modulation and performance would imply that degree of change in functional connectivity is accompanied by higher accuracy score, which may not be the case. Instead, our reasoning is based on the fact that the main thing happening between the pre- and post-encoding scans was the memory encoding. While this does not guarantee that pre-post differences represent memory consolidation processes, we believe it is one reasonable interpretation of the within-subject effects observed, even without a direct between-subject correlation with performance. Moreover, we can still point to several indicators from our data supporting an interpretation of our post-encoding findings in line with early systems consolidation. Most prominent is the similarity with hippocampus-centered encoding patterns, considered the "hallmark" of reactivation (Hoffman and McNaughton 2002; O'Neill et al. 2010; Tambini and Davachi 2019). When analyzed separately, both the first and second half of the immediate post-encoding rest showed the same pattern of hippocampal rsFC upregulation compared to baseline as when combined, hence the post-encoding effects were not driven by the first few minutes after encoding. Also, the disproportionate increase in hippocampal centrality, relative to all other investigated subcortical and neocortical nodes, indicates strong post-encoding relevance of this core structure for episodic memory formation. To some extent this hippocampal selectivity also points against a pure Hebbian mechanism—sustained novelty-induced neuronal reverberations (Ribeiro et al. 2004)—behind the current findings as it is unclear why this process should prioritize hippocampal edges. Finally, our observation of increased post-encoding functional connectivity between thalamus and core DMN nodes, and the covarying relationship between thalamus–DMN and hippocampal connectivity mediated by the hippocampus–thalamus coupling fits well with recent models of thalamic enabling of low-interference states during hippocampally orchestrated memory reactivation (Wagner et al. 2019; Yang et al. 2019; Higgins et al. 2021).

The observed change in hippocampal coupling could be due to other cognitive functions or general task processing, not specifically related to memory. Also, our task is an intentional multimodal task, including visual and auditory stimuli, which could lead to a broader or different activation than after a unimodal or implicit learning task. Including control conditions with implicit learning scenarios, a task with similar task demands but no requirement for memorizing stimuli and memory tasks with different degree of task demands could help resolve this debate in future studies.

In contrast to the current findings, a recent study by Cowan et al. (2021), also focusing on hippocampal post-encoding modulations, only observed a limited increase in hippocampal–parahippocampal FC. However, their pre-encoding rest period followed an extensive familiarization task; thus, the baseline conditions were not directly comparable to the current task. The role of task design and the temporal nature of the rsFC changes need more systematic testing in the future.

We did not observe any age effects on hippocampal post-encoding modulations. Although this was contrary to our expectations, it suggests that the upregulation of hippocampal–neocortical connectivity after intensive memory encoding represents a general phenomenon seen across the adult lifespan. Nevertheless, we believe that future studies should continue pursuing this link; one of the most characteristic changes occurring in human cognition with higher age is the decline of episodic memory function (Nyberg et al. 2012), but descriptions of awake systems consolidation in samples other than young adults are almost completely absent in the literature (see (Kukolja et al. 2016) for a notable exception). While we did not observe age differences in awake post-encoding rest periods, there are some indications that sleep-dependent memory consolidation is affected by age (Harand et al. 2012) and future investigations could benefit from combining fMRI and sleep assessments.

Conclusion

In the present study, we show that the coupling between hippocampus and the neocortex is upregulated nearly globally during post-encoding awake rest. The spatial configuration of these modulations resembles hippocampal connectivity seen during active encoding, indicating continuation of the hippocampal encoding state into stimulus-free periods. Such systems-wide encoding reinstatement at rest suggests reactivation of memory traces involves aspects beyond perceptual characteristics of encoded events. We did not observe any age effects on hippocampal post-encoding modulation; hence the upregulation seems to be age invariant.

Supplementary material

Supplementary material is available at *Cerebral Cortex* online.

Acknowledgments

We thank Prof. Lars Nyberg for helpful comments on the manuscript. We thank all the participants for their time and effort and our colleagues in LCBC, especially Marie Strømstad, for contributing to data collection.

Funding

This work was supported by The European Research Council (283634, 725025 to AMF and 313440 to KBW) and Norwegian Research Council (to A.M.F. and K.B.W.).

Conflict of interest statement: The authors declare no conflict of interest.

References

Abraham A, Pedregosa F, Eickenberg M, Gervais P, Mueller A, Kossaifi J, Gramfort A, Thirion B, Varoquaux G. Machine learning for neuroimaging with scikit-learn. *Front Neuroinform*. 2014: 8:14.

Aggleton JP, Pralus A, Nelson AJD, Hornberger M. Thalamic pathology and memory loss in early Alzheimer's disease: moving the focus from the medial temporal lobe to Papez circuit. *Brain*. 2016:139(7): 1877–1890.

Alvarez P, Squire LR. Memory consolidation and the medial temporal lobe: a simple network model. *PNAS*. 1994:91(15):7041–7045.

Andersson JLR, Skare S, Ashburner J. How to correct susceptibility distortions in spin-echo echo-planar images: application to diffusion tensor imaging. *NeuroImage*. 2003:20(2):870–888.

Bates D, Mächler M, Bolker B, Walker S. Fitting linear mixed-effects models using lme4. *J Stat Softw*. 2015:67(1):1–48.

Beason-Held LL, Shafer AT, Goh JO, Landman BA, Davatzikos C, Viscomi B, Ash J, Kitner-Triolo M, Ferrucci L, Resnick SM. Hippocampal activation and connectivity in the aging brain. *Brain Imaging Behav*. 2021:15(2):711–726.

Beck AT, Steer RA, Carbin MG. Psychometric properties of the Beck Depression Inventory: twenty-five years of evaluation. *Clin Psychol Rev*. 1988:8(1):77–100.

Benjamini Y, Hochberg Y. Controlling the false discovery rate: a practical and powerful approach to multiple testing. *J R Stat Soc B Methodol*. 1995:57(1):289–300.

Brodeur MB, Dionne-Dostie E, Montreuil T, Lepage M. The Bank of Standardized Stimuli (BOSS), a new set of 480 normative photos of objects to be used as visual stimuli in cognitive research. *PLoS One*. 2010:5(5):e10773.

Buch ER, Claudino L, Quentin R, Bönstrup M, Cohen LG. Consolidation of human skill linked to waking hippocampo-neocortical replay. *Cell Rep*. 2021:35(10):109193.

Burt JB, Helmer M, Shinn M, Anticevic A, Murray JD. Generative modeling of brain maps with spatial autocorrelation. *NeuroImage*. 2020:220:117038.

Buzsáki G. Hippocampal sharp wave-ripple: a cognitive biomarker for episodic memory and planning. *Hippocampus*. 2015:25(10):1073–1188.

Carr MF, Jadhav SP, Frank LM. Hippocampal replay in the awake state: a potential substrate for memory consolidation and retrieval. *Nat Neurosci*. 2011:14(2):147–153.

Chelnokova O, Laeng B, Eikemo M, Riegels J, Løseth G, Maurud H, Willoch F, Leknes S. Rewards of beauty: the opioid system mediates social motivation in humans. *Mol Psychiatry*. 2014:19(7):746–747.

Cooper RA, Ritchey M. Cortico-hippocampal network connections support the multidimensional quality of episodic memory. *elife*. 2019:8:e45591.

Cowan ET, Fain M, O'Shea I, Ellman LM, Murty VP. VTA and anterior hippocampus target dissociable neocortical networks for post-novelty enhancements. *J Neurosci*. 2021:41(38):8040–8050.

de Voogd LD, Fernández G, Hermans EJ. Awake reactivation of emotional memory traces through hippocampal–neocortical interactions. *NeuroImage*. 2016:134:563–572.

Deuker L, Olligs J, Fell J, Kranz TA, Mormann F, Montag C, Reuter M, Elger CE, Axmacher N. Memory consolidation by replay of stimulus-specific neural activity. *J Neurosci*. 2013:33(49):19373–19383.

Di X, Biswal BB. Toward task connectomics: examining whole-brain task modulated connectivity in different task domains. *Cereb Cortex*. 2019:29(4):1572–1583.

Di X, Reynolds RC, Biswal BB. Imperfect (de)convolution may introduce spurious psychophysiological interactions and how to avoid it. *Hum Brain Mapp*. 2017:38(4):1723–1740.

Epstein R, Kanwisher N. A cortical representation of the local visual environment. *Nature*. 1998:392(6676):598–601.

Esteban O, Birman D, Schaer M, Koyejo OO, Poldrack RA, Gorgolewski KJ. MRIQC: advancing the automatic prediction of image quality in MRI from unseen sites. *PLoS One*. 2017:12(9):e0184661.

Esteban O, Markiewicz CJ, Blair RW, Moodie CA, Isik AI, Erramuzpe A, Kent JD, Goncalves M, DuPre E, Snyder M, et al. fMRIPrep: a robust preprocessing pipeline for functional MRI. *Nat Methods*. 2019:16(1):111–116.

Fischl B, Salat DH, Busa E, Albert M, Dieterich M, Haselgrove C, van der Kouwe A, Killiany R, Kennedy D, Klaveness S, et al. Whole brain segmentation: automated labeling of neuroanatomical structures in the human brain. *Neuron*. 2002:33(3):341–355.

Fjell AM, Sneve MH, Storsve AB, Grydeland H, Yendiki A, Walhovd KB. Brain events underlying episodic memory changes in aging: a longitudinal investigation of structural and functional connectivity. *Cereb Cortex*. 2016:26(3):1272–1286.

Folstein MF, Folstein SE, McHugh PR. "Mini-mental state": a practical method for grading the cognitive state of patients for the clinician. *J Psychiatr Res*. 1975:12(3):189–198.

Fornito A, Zalesky A, Bullmore ET, editors. Chapter 4 - node degree and strength. In: *Fundamentals of brain network analysis*. San Diego: Academic Press; 2016. pp. 115–136

Foster DJ. Replay comes of age. *Annu Rev Neurosci*. 2017:40(1):581–602.

Gitelman DR, Penny WD, Ashburner J, Friston KJ. Modeling regional and psychophysiologic interactions in fMRI: the importance of hemodynamic deconvolution. *NeuroImage*. 2003:19(1):200–207.

Gorgolewski K, Burns C, Madison C, Clark D, Halchenko Y, Waskom M, Ghosh S. Nipype: a flexible, lightweight and extensible neuroimaging data processing framework in python. *Front Neuroinform*. 2011:5:13.

Grill-Spector K, Kourtzi Z, Kanwisher N. The lateral occipital complex and its role in object recognition. *Vis Res*. 2001:41(10–11):1409–1422.

Gruber MJ, Ritchey M, Wang S-F, Doss MK, Ranganath C. Post-learning hippocampal dynamics promote preferential retention of rewarding events. *Neuron*. 2016:89(5):1110–1120.

Harand C, Bertran F, Doidy F, Guénolé F, Desgranges B, Eustache F, Rauchs G. How aging affects sleep-dependent memory consolidation? *Front Neurol*. 2012:3:8.

Higgins C, Liu Y, Vidaurre D, Kurth-Nelson Z, Dolan R, Behrens T, Woolrich M. Replay bursts in humans coincide with activation of the default mode and parietal alpha networks. *Neuron*. 2021:109(5):882–893.e7.

Hoffman KL, McNaughton BL. Coordinated reactivation of distributed memory traces in primate neocortex. *Science*. 2002:297(5589):2070–2073.

Jacobacci F, Armony JL, Yeffal A, Lerner G, Amaro E, Jovicich J, Doyon J, Della-Maggiore V. Rapid hippocampal plasticity supports motor sequence learning. *Proc Natl Acad Sci U S A*. 2020:117(38):23898–23903.

Kanwisher N, McDermott J, Chun MM. The fusiform face area: a module in human extrastriate cortex specialized for face perception. *J Neurosci*. 1997:17(11):4302–4311.

Kaplan R, Adhikari MH, Hindriks R, Mantini D, Murayama Y, Logothetis NK, Deco G. Hippocampal sharp-wave ripples influence selective activation of the default mode network. *Curr Biol*. 2016:26(5):686–691.

Kim H. Neural activity that predicts subsequent memory and forgetting: a meta-analysis of 74 fMRI studies. *NeuroImage*. 2011:54(3):2446–2461.

King DR, de Chastelaine M, Rugg MD. Recollection-related increases in functional connectivity across the healthy adult lifespan. *Neurobiol Aging*. 2018:62:1–19.

Kukolja J, Göreci DY, Onur ÖA, Riedl V, Fink GR. Resting-state fMRI evidence for early episodic memory consolidation: effects of age. *Neurobiol Aging*. 2016:45:197–211.

Kurth-Nelson Z, Economides M, Dolan RJ, Dayan P. Fast sequences of non-spatial state representations in humans. *Neuron*. 2016:91(1):194–204.

Kuznetsova A, Brockhoff PB, Christensen RHB. lmerTestPackage: tests in linear mixed effects models. *J Stat Softw*. 2017:82(13):1–26.

Lindquist MA, Geuter S, Wager TD, Caffo BS. Modular preprocessing pipelines can reintroduce artifacts into fMRI data. *Hum Brain Mapp*. 2019:40(8):2358–2376.

Liu Y, Dolan RJ, Kurth-Nelson Z, Behrens TEJ. Human replay spontaneously reorganizes experience. *Cell*. 2019:178(3):640–652.e14.

Logothetis NK, Eschenko O, Murayama Y, Augath M, Steudel T, Evrard HC, Besserve M, Oeltermann A. Hippocampal–cortical interaction during periods of subcortical silence. *Nature*. 2012:491(7425):547–553.

Margulies DS, Falkiewicz M, Huntenburg JM. A cortical surface-based geodesic distance package for Python. *GigaScience*. 2016:5(suppl_1):s13742-016-0147-0-q.

Maus B, van Breukelen GJP, Goebel R, Berger MPF. Optimization of blocked designs in fMRI studies. *Psychometrika*. 2010:75(2):373–390.

McCormick C, Moscovitch M, Protzner AB, Huber CG, McAndrews MP. Hippocampal–neocortical networks differ during encoding and retrieval of relational memory: functional and effective connectivity analyses. *Neuropsychologia*. 2010:48(11):3272–3281.

McLaren DG, Ries ML, Xu G, Johnson SC. A generalized form of context-dependent psychophysiological interactions (gPPI): a comparison to standard approaches. *NeuroImage*. 2012:61(4):1277–1286.

Murty VP, Tompary A, Adcock RA, Davachi L. Selectivity in postencoding connectivity with high-level visual cortex is associated with reward-motivated memory. *J Neurosci*. 2017:37(3):537–545.

Murty VP, DuBrow S, Davachi L. Decision-making increases episodic memory via postencoding consolidation. *J Cogn Neurosci*. 2019:31(9):1308–1317.

Nadel L, Moscovitch M. Memory consolidation, retrograde amnesia and the hippocampal complex. *Curr Opin Neurobiol*. 1997:7(2):217–227.

Ness HT, Folvik L, Sneve MH, Vidal-Piñeiro D, Raud L, Geier OM, Nyberg L, Walhovd KB, Fjell AM. Reduced hippocampal-striatal interactions during formation of durable episodic memories in aging. *Cereb Cortex*. 2021:32(11):2358–2372.

Nyberg L, Lövdén M, Riklund K, Lindenberger U, Bäckman L. Memory aging and brain maintenance. *Trends Cogn Sci*. 2012:16(5):292–305.

O'Neill J, Pleydell-Bouverie B, Dupret D, Csicsvari J. Play it again: reactivation of waking experience and memory. *Trends Neurosci*. 2010:33(5):220–229.

Olman CA, Davachi L, Inati S. Distortion and signal loss in medial temporal lobe. *PLoS One*. 2009:4(12):e8160.

Pedregosa F, Varoquaux G, Gramfort A, Michel V, Thirion B, Grisel O, Blondel M, Prettenhofer P, Weiss R, Dubourg V, et al. Scikit-learn: machine learning in python. *J Mach Learn Res*. 2011:12:2825–2830.

Poppenk J, Evensmoen HR, Moscovitch M, Nadel L. Long-axis specialization of the human hippocampus. *Trends Cogn Sci*. 2013:17(5):230–240.

Pruim RHR, Mennes M, van Rooij D, Llera A, Buitelaar JK, Beckmann CF. ICA-AROMA: a robust ICA-based strategy for removing motion artifacts from fMRI data. *NeuroImage*. 2015:112:267–277.

R Core Team. *R: A language and environment for statistical computing*. Vienna, Austria: R Foundation for Statistical Computing; 2022. https://www.R-project.org/.

Ribeiro S, Gervasoni D, Soares ES, Zhou Y, Lin S-C, Pantoja J, Lavine M, Nicolelis MAL. Long-lasting novelty-induced neuronal reverberation during slow-wave sleep in multiple forebrain areas. *PLoS Biol*. 2004:2(1):e24.

Schaefer A, Kong R, Gordon EM, Laumann TO, Zuo X-N, Holmes AJ, Eickhoff SB, Yeo BTT. Local-global parcellation of the human cerebral cortex from intrinsic functional connectivity MRI. *Cereb Cortex*. 2018:28(9):3095–3114.

Schapiro AC, McDevitt EA, Rogers TT, Mednick SC, Norman KA. Human hippocampal replay during rest prioritizes weakly learned information and predicts memory performance. *Nat Commun*. 2018:9(1):3920.

Schlichting ML, Preston AR. Memory reactivation during rest supports upcoming learning of related content. *PNAS*. 2014:111(44):15845–15850.

Schlichting ML, Preston AR. Hippocampal–medial prefrontal circuit supports memory updating during learning and post-encoding rest. *Neurobiol Learn Mem*. 2016:134:91–106.

Sneve MH, Grydeland H, Nyberg L, Bowles B, Amlien IK, Langnes E, Walhovd KB, Fjell AM. Mechanisms underlying encoding of short-lived versus durable episodic memories. *J Neurosci*. 2015:35(13):5202–5212.

Staresina BP, Alink A, Kriegeskorte N, Henson RN. Awake reactivation predicts memory in humans. *Proc Natl Acad Sci*. 2013:110(52):21159–21164.

Tambini A, Davachi L. Awake reactivation of prior experiences consolidates memories and biases cognition. *Trends Cogn Sci*. 2019:23(10):876–890.

Tambini A, Ketz N, Davachi L. Enhanced brain correlations during rest are related to memory for recent experiences. *Neuron*. 2010:65(2):280–290.

Tang L, Pruitt PJ, Yu Q, Homayouni R, Daugherty AM, Damoiseaux JS, Ofen N. Differential functional connectivity in anterior and posterior hippocampus supporting the development of memory formation. *Front Hum Neurosci*. 2020:14:204.

Thomas Yeo BT, Krienen FM, Sepulcre J, Sabuncu MR, Lashkari D, Hollinshead M, Roffman JL, Smoller JW, Zöllei L, Polimeni JR, et al. The organization of the human cerebral cortex estimated by intrinsic functional connectivity. *J Neurophysiol*. 2011:106(3):1125–1165.

Tompary A, Davachi L. Consolidation promotes the emergence of representational overlap in the hippocampus and medial prefrontal cortex. *Neuron*. 2017:96(1):228–241.e5.

Tong Y, Hocke LM, Frederick BB. Low frequency systemic hemodynamic "noise" in resting state BOLD fMRI: characteristics, causes, implications, mitigation strategies, and applications. *Front Neurosci*. 2019:13:787. doi: https://doi.org/10.3389/fnins.2019.00787.

Vallat R. Pingouin: statistics in python. *J Open Source Softw*. 2018:3(31):1026.

van Kesteren MTR, Fernández G, Norris DG, Hermans EJ. Persistent schema-dependent hippocampal-neocortical connectivity during memory encoding and postencoding rest in humans. *PNAS*. 2010:107(16):7550–7555.

Wagner IC, van Buuren M, Fernández G. Thalamo-cortical coupling during encoding and consolidation is linked to durable memory formation. *NeuroImage*. 2019:197:80–92.

Wechsler D. *Wechsler abbreviated scale of intelligence*. New York, NY: The Psychological Corporation: Harcourt Brace & Company; 1999.

Westphal AJ, Wang S, Rissman J. Episodic memory retrieval benefits from a less modular brain network organization. *J Neurosci*. 2017:37(13):3523–3531.

Yang M, Logothetis NK, Eschenko O. Occurrence of hippocampal ripples is associated with activity suppression in the mediodorsal thalamic nucleus. *J Neurosci*. 2019:39(3):434–444.

Yesavage JA, Brink TL, Rose TL, Lum O, Huang V, Adey M, Leirer VO. Development and validation of a geriatric depression screening scale: a preliminary report. *J Psychiatr Res*. 1982:17(1):37–49.